

# Proton-Coupled Electron Transfer and Adduct Configuration Are Important for C4a-Hydroperoxyflavin Formation and Stabilization in a Flavoenzyme

Thanyaporn Wongnate,<sup>†,‡</sup> Panida Surawatanawong,<sup>§,‡</sup> Surawit Visitsatthawong,<sup>§</sup> Jeerus Sucharitakul,<sup>||</sup> Nigel S. Scrutton,<sup>†</sup> and Pimchai Chaiyen\*,<sup>†</sup>

<sup>†</sup>Department of Biochemistry and Center of Excellence in Protein Structure and Function, Faculty of Science, Mahidol University, Bangkok, 10400 Thailand

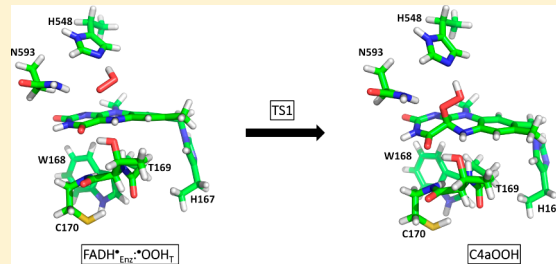
<sup>§</sup>Department of Chemistry and Center of Excellence for Innovation in Chemistry, Mahidol University, Bangkok 10400 Thailand

<sup>||</sup>Department of Biochemistry, Faculty of Dentistry, Chulalongkorn University, Henri-Dunant Road, Patumwan, Bangkok, 10300 Thailand

<sup>†</sup>Manchester Institute of Biotechnology and Faculty of Life Sciences, The University of Manchester, Manchester M1 7DN United Kingdom

## S Supporting Information

**ABSTRACT:** Determination of the mechanism of dioxygen activation by flavoenzymes remains one of the most challenging problems in flavoenzymology for which the underlying theoretical basis is not well understood. Here, the reaction of reduced flavin and dioxygen catalyzed by pyranose 2-oxidase (P2O), a flavoenzyme oxidase that is unique in its formation of C4a-hydroperoxyflavin, was investigated by density functional calculations, transient kinetics, and site-directed mutagenesis. Based on work from the 1970s–1980s, the current understanding of the dioxygen activation process in flavoenzymes is believed to involve electron transfer from flavin to dioxygen and subsequent proton transfer to form C4a-hydroperoxyflavin. Our findings suggest that the first step of the P2O reaction is a single electron transfer coupled with a proton transfer from the conserved residue, His548. In fact, proton transfer enhances the electron acceptor ability of dioxygen. The resulting ·OOH of the open-shell diradical pair is placed in an optimal position for the formation of C4a-hydroperoxyflavin. Furthermore, the C4a-hydroperoxyflavin is stabilized by the side chains of Thr169, His548, and Asn593 in a “face-on” configuration where it can undergo a unimolecular reaction to generate H<sub>2</sub>O<sub>2</sub> and oxidized flavin. The computational results are consistent with kinetic studies of variant forms of P2O altered at residues Thr169, His548, and Asn593, and kinetic isotope effects and pH-dependence studies of the wild-type enzyme. In addition, the calculated energy barrier is in agreement with the experimental enthalpy barrier obtained from Eyring plots. This work revealed new insights into the reaction of reduced flavin with dioxygen, demonstrating that the positively charged residue (His548) plays a significant role in catalysis by providing a proton for a proton-coupled electron transfer in dioxygen activation. The interaction around the NS-position of the C4a-hydroperoxyflavin is important for dictating the stability of the intermediate.



## INTRODUCTION

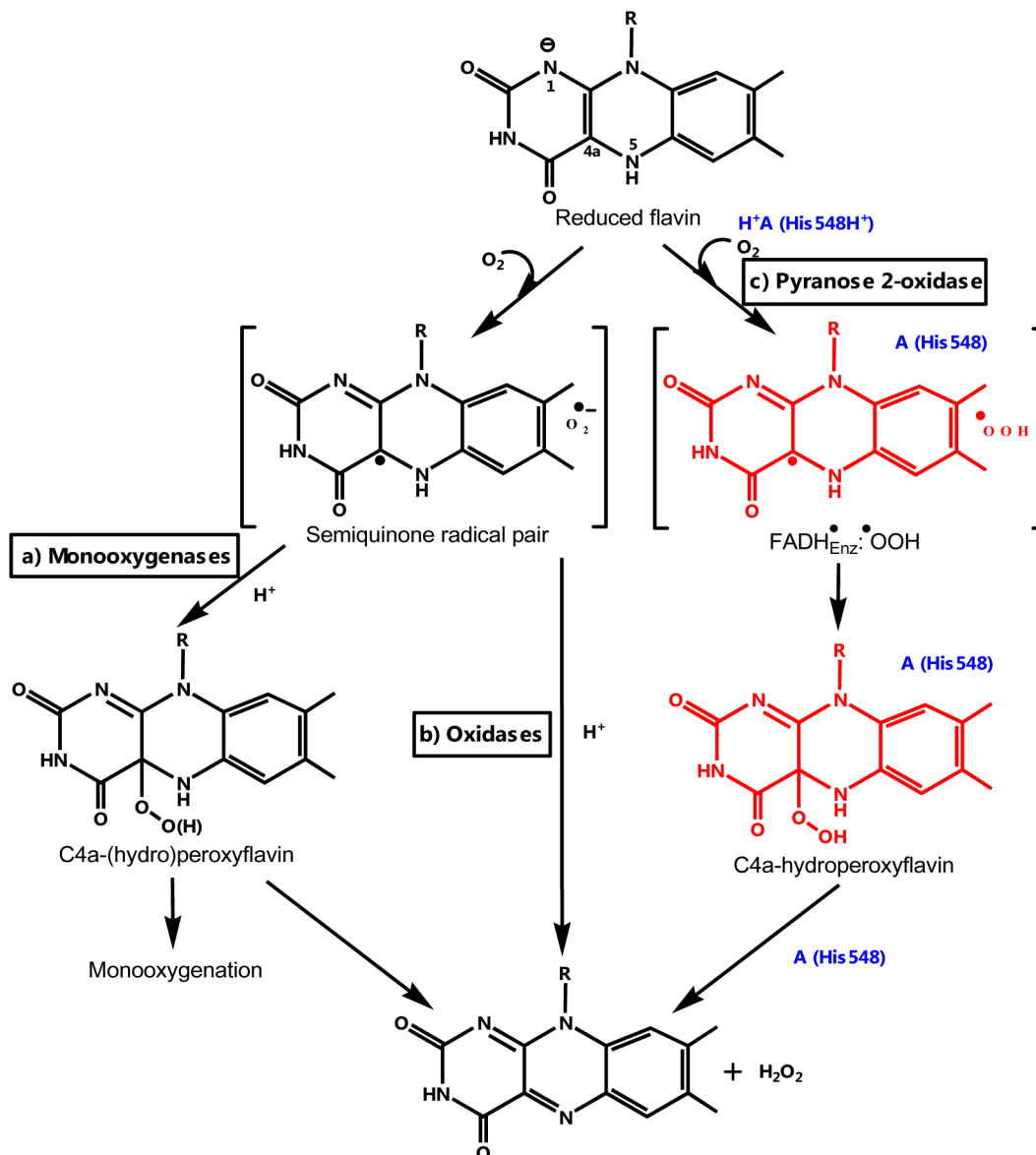
Flavoenzymes not only have indispensable roles in cellular metabolism<sup>1</sup> but also are useful as biocatalysts for chemical synthesis reactions and as bioelectrocatalysts for biofuel cell applications.<sup>2,3</sup> Baeyer–Villiger monooxygenase has been used widely in pharmaceutical industries to synthesize drugs.<sup>4</sup> Recently, flavin derivatives were successfully used for catalytic water oxidation in a photochemical water splitting process.<sup>3</sup> Therefore, understanding how flavoenzymes function is crucial to improving their applications and to developing biomimetic flavin derivatives for use as efficient biocatalysts and biosensors and in biofuel cells.<sup>5</sup>

The physical and chemical basis underlying the reactions of reduced flavin and dioxygen in flavoenzymes is one of the most

fascinating issues in flavoenzymology.<sup>6</sup> The same reduced flavin (FAD or FMN) when bound to different proteins reacts differently with dioxygen (i.e., to form H<sub>2</sub>O<sub>2</sub> in oxidases, to form C4a-(hydro)peroxyflavin in monooxygenases, or to have sluggish reactivity toward dioxygen in dehydrogenases in order to transfer electrons to other acceptors). The different reaction outcomes due to the different active site environments of these proteins allow nature to use the same set of chemical reactants to perform a variety of flavoenzyme functions, including use of the abundant oxygen in aerobic systems as an electron acceptor (oxidase), to incorporate an oxygen atom into an organic

Received: August 30, 2013

Published: December 16, 2013

Scheme 1. Flavin Reaction Mechanisms with Dioxygen<sup>a</sup>

<sup>a</sup>Paths (a) and path (b) are conventional pathways for the reactions with O<sub>2</sub> in monooxygenases and oxidases, respectively. Path (c) is the alternative pathway for the reactions with O<sub>2</sub> in pyranose 2-oxidase, according to the findings of the current study.

substrate (monooxygenase), or to mediate electron transfer in complex protein systems (dehydrogenase). Most of our current understanding of flavin chemistry in flavoenzymes is based on work performed in the 1970s–1980s by Bruice et al.<sup>7,8</sup> and Massey et al.,<sup>9</sup> and the current view of the reaction of reduced flavin with oxygen in oxidases and oxygenases can be summarized as depicted in Scheme 1 (paths a and b).

In chemical synthesis, catalytic oxidative reactions and oxygen insertions with high selectivity generally require multiple steps and often require heavy metals. Flavin is among a few organic cofactors that can use molecular oxygen for oxygenation reactions.<sup>5</sup> The mechanism for the control of this reaction should be well coordinated so that leakage of hazardous reactive oxygen species during enzyme turnover is minimized and the oxygenases can most efficiently catalyze oxygenation. Many research groups in the past recent years have investigated the role of active site residues that are important for dioxygen activation.<sup>10–17</sup> One of the recurrent

features found in these systems is the presence of a positively charged residue that is located near the flavin N5. Previous work suggested that this positive charge provides a preorganized environment that stabilizes the superoxide anion species<sup>10–14,16</sup> that forms after the first step of electron transfer (path a and b in Scheme 1).<sup>8</sup> However, the electronic structures and energies of key intermediates in the dioxygen activation mechanisms have not been studied in detail.

Pyranose 2-oxidase (P2O) is a suitable flavoenzyme for exploring dioxygen activation and C4a-hydroperoxyflavin stabilization. P2O catalyzes the oxidation of pyranose sugars to form 2-keto-sugars and H<sub>2</sub>O<sub>2</sub> (Scheme S1, Supporting Information [SI]). The enzyme has been applied in the synthesis of rare sugars.<sup>2</sup> Thus far, it has been the only flavoenzyme oxidase, in which C4a-hydroperoxyflavin has been detected as an intermediate under natural turnover conditions.<sup>18,19</sup> The reaction of P2O could be viewed as a missing link in evolution connecting flavin-dependent monooxygenases

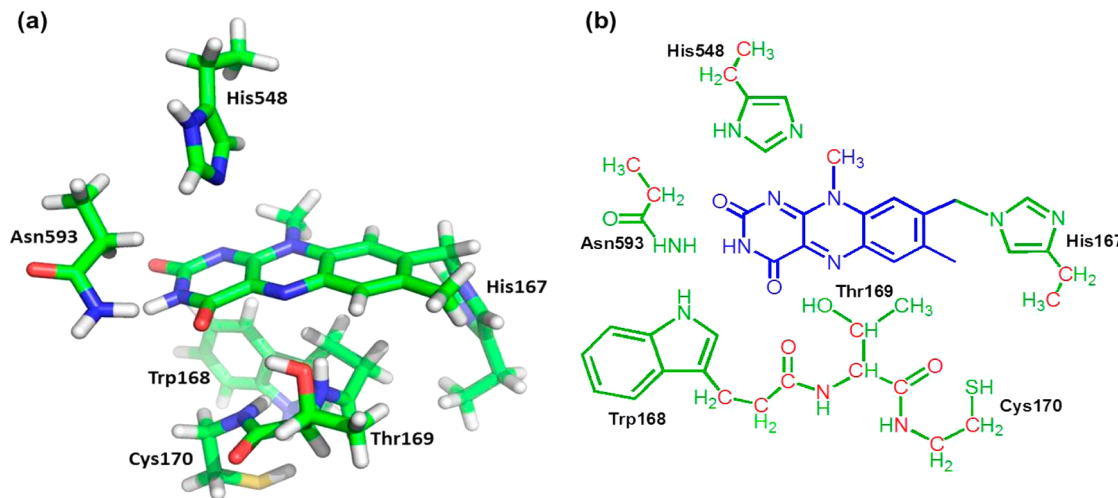


**Figure 1.** Active site model of P2O(WT) in the closed conformation. (a) X-ray structure of the active site model. (b) Schematic representation of the active site model. The isoalloxazine ring of FAD is shown in blue, flexible residues in green, and constrained atoms in red.

in which formation of C4a(hydro)peroxyflavin is mandatory and flavoenzyme oxidases in which formation of C4a-hydroperoxyflavin is possibly just one of the means of generating  $\text{H}_2\text{O}_2$  (Scheme 1). As no X-ray structure of enzyme-bound C4a-hydroperoxyflavin is available, it remains elusive how the intermediate is stabilized in flavoenzymes. It has been proposed that a cavity that is commonly found above the flavin C4a atom of monooxygenases may serve as an entrance for oxygen diffusion and accommodate the peroxide adduct.<sup>6</sup>

Theoretical calculations have been used to study electronic structures and energies in enzymatic reactions.<sup>20–23</sup> Reaction mechanisms have been theoretically investigated for a few flavoenzymes, e.g., a Baeyer–Villiger monooxygenase (oxygen insertion<sup>24</sup>), *p*-hydroxybenzoate hydroxylase and phenol hydroxylase (aromatic hydroxylation<sup>25,26</sup>), 2-methyl-3-hydroxypyridine-5-carboxylate monooxygenase (ring-cleavage reaction<sup>27,28</sup>), BluB (cleavage of riboflavin<sup>29</sup>), glucose 1-oxidase and aryl alcohol oxidase (oxidation of alcohol moiety<sup>30,31</sup>). The mechanisms of  $\text{H}_2\text{O}_2$  elimination from a free C4a-hydroperoxyflavin species was recently investigated by Bach and Mattevi.<sup>32</sup> In combination with experimental data, computational studies can provide greater insights on the enzyme mechanisms.<sup>20</sup>

In this report, the reaction of reduced flavin and dioxygen catalyzed by P2O was explored using density functional theory (DFT). The calculated activation energies were compared to the experimental activation enthalpies determined from the Eyring plot based on transient kinetic studies at various temperatures. The calculations agreed well with the results from kinetic isotope effect (KIE) and site-directed mutagenesis studies. DFT analysis gave the following new insights into this reaction: (i) the protonated His548 does not stabilize the superoxide anion via electrostatic interactions; rather, it acts as a general acid by providing a proton for the proton-coupled electron transfer in dioxygen activation (path c in Scheme 1) and (ii) the  $-\text{OOH}$  moiety of C4a-hydroperoxyflavin is in the “face-on” configuration and stabilized by a hydrogen-bonding network from His548, Asn593, and Thr169.

## EXPERIMENTAL PROCEDURES

**Computational Details.** All calculations were performed with the Gaussian 09 program.<sup>33</sup> B3LYP<sup>34–36</sup> functional has been shown to be suitable for the study of enzymatic reactions.<sup>29,37,38</sup> Thus, B3LYP was used for all geometry optimizations and frequency calculations in this study. The 6-31++G(d,p)<sup>39–41</sup> basis set was used for the H that forms  $\text{H}_2\text{O}_2$  and 6-31G(d) was used for all other atoms.<sup>39–41</sup> The single-point energy and solvation free energy corrections were calculated by B3LYP/6-311+G(d,p) on the geometries based on the gas-phase optimizations using the conductor-like polarizable continuum model (CPCM)<sup>42</sup> with UAKS<sup>43</sup> atomic radii and a dielectric constant of 4.0 to represent the protein environment. The energy barrier based on the electronic energy with solvation correction obtained from B3LYP/6-311+G(d,p) calculations is lower than the electronic energy obtained from B3LYP/6-31G(d) calculations, especially for the  $\text{H}_2\text{O}_2$  elimination step (Table S1, SI). Open-shell systems were treated using spin unrestricted B3LYP (UB3LYP).

The active site model was taken from the crystal structure of P2O(WT) in the closed conformation (1.80 Å; PDB code: 1TT0).<sup>44</sup> The model consists of 118 atoms, which includes  $\text{FADH}^-$  (the isoalloxazine part) and the residues within ~5 Å radius from the N5 atom of the  $\text{FADH}^-$  (Trp168, Thr169, and Cys170) and the key conserved residues<sup>45</sup> (His167, His548, and Asn593) of the enzyme (Figure 1). To minimize the computational power for the relevant protein environment, only the side chains were allowed to be flexible during the geometry optimization. Thus, the atoms on the backbone were constrained at the initial positions in the crystal structure to maintain a reasonable geometry of the active site while all other atoms were optimized (Figure 1). For transition states, frequencies were calculated to ensure that there was one imaginary frequency corresponding to the reaction coordinate. Note that, since some atoms in the model are constrained during optimization, the intermediate and transition state structures are not strictly stationary points. Thus, the zero-point vibrational energy corrections and thermal effects are not well-defined and are not considered in this study.

To critically evaluate the extent of spin contamination in open-shell species, the expectation value for the total spin angular momentum,  $\langle S^2 \rangle$ , of all diradical species in this study were calculated and are shown in Table S2 in SI. The data indicate that, for the triplet species, there is no significant problem with the spin contamination as all of the  $\langle S^2 \rangle_{\text{triplet}}$  values are close to 2. For the open-shell singlet species, the  $\langle S^2 \rangle_{\text{singlet}}$  values are close to 1 and largely differ from zero. This may be because the use of the broken symmetry approach to calculate the open-shell singlet species can result in spin contamination from higher spin states. As the spin projection (SP) technique was successfully employed in the calculation of diradical energies in previous works,<sup>29,46</sup> we used this method to estimate the energy of the spin-

unrestricted open-shell singlet species (eqs 1, 2).<sup>46</sup>  $E^X$  is the electronic energy, and  $\langle S^2 \rangle^X$  is the expectation value for the total spin angular momentum of the spin state X (X = singlet or triplet).<sup>46</sup>

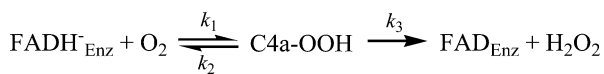
$$E_{SP}^{\text{singlet}} = E^{\text{singlet}} + C_{SC}[E^{\text{singlet}} - E^{\text{triplet}}] \quad (1)$$

$$C_{SC} = \frac{\langle S^2 \rangle^{\text{singlet}}}{\langle S^2 \rangle^{\text{triplet}} - \langle S^2 \rangle^{\text{singlet}}} \quad (2)$$

**Temperature Dependence Studies.** The measurements were performed using a TgK Scientific model SF-61DX stopped-flow spectrophotometer in single-mixing mode. The optical path length of the observation cell was 1 cm. The experimental protocols used were similar to those in a previous report.<sup>18,47,48</sup> In brief, the stopped-flow apparatus was made anaerobic by flushing the flow system with an anaerobic buffer containing 10 mM sodium dithionite in 50 mM sodium phosphate buffer, pH 7.0. The buffer was made anaerobic by equilibrating with oxygen-free nitrogen (ultrahigh purity) that had been passed through an Oxyclear oxygen removal column (Labclear). The anaerobic buffer was allowed to stand in the flow system overnight. The flow unit was then rinsed with the anaerobic buffer before experiments. For studying the oxidative half-reaction, an anaerobic enzyme solution was equilibrated in an anaerobic glovebox (Belle Technology). The enzyme was then reduced with a solution of 10 mM D-glucose in 100 mM sodium phosphate buffer pH 7.0. While adding the solution of D-glucose, enzyme spectra were recorded using a spectrophotometer inside the glovebox to ensure complete reduction. The reduced enzyme solution was placed in a glass tonometer and loaded onto the stopped-flow spectrophotometer.

Reduced P2O(WT) (53 μM) was mixed with buffers containing 1.22 mM O<sub>2</sub> (concentrations before mixing) at various temperatures (5, 10, 15, 20, 25, and 30 °C) in a stopped-flow spectrophotometer. Large amplitude changes were detected at 395 and 458 nm. The reaction showed two kinetic phases. For example, at 5 °C, the first phase (0.002–0.04 s, increase of absorbance at 395 nm) indicates the formation of a C4a-hydroperoxyflavin intermediate that subsequently decays in the second phase (0.04–1 s) to yield H<sub>2</sub>O<sub>2</sub> and the oxidized enzyme. The second phase occurred simultaneously with an absorbance increase at 458 nm (Figure 5).<sup>18,49,50</sup> Apparent rate constants ( $k_{\text{obs}}$ ) were calculated from the kinetic traces using exponential fits and the software packages Kinetic Studio (TgK Scientific, Bradford-on-Avon, UK) or Program A (developed by R. Chang, C.-J. Chiu, J. Dinverno, and D. P. Ballou, at University of Michigan, Ann Arbor, MI). Simulations were performed by numerical methods with Runge–Kutta algorithms implemented in Berkeley Madonna 8.3 with a time step of 10<sup>-3</sup> s. Rate constants associated with Scheme 2 can be analyzed according to eqs 3 and 4.<sup>18</sup> Analysis yielded

**Scheme 2. Reaction Mechanism of the Oxidative Half-Reaction of P2O(WT)**



a bimolecular rate constant for the formation of C4a-hydroperoxyflavin ( $k_1$ ), a reverse rate constant ( $k_2$ ), and a rate constant for H<sub>2</sub>O<sub>2</sub> elimination ( $k_3$ ). A summary of the rate constants is provided in Table S4 in SI. The rate constants ( $k_1$ ,  $k_2$ , and  $k_3$ ) were plotted against the temperature used (see Figure S5, SI).

$$k_{\text{obs1}} = k_1[\text{O}_2] + k_2 + k_3 - \frac{k_1 k_3 [\text{O}_2]}{k_1[\text{O}_2] + k_2 + k_3} \quad (3)$$

$$k_{\text{obs2}} = \frac{k_1 k_3 [\text{O}_2]}{k_1[\text{O}_2] + k_2 + k_3} \quad (4)$$

The Eyring equation was used for determining the enthalpy of activation ( $\Delta H^\ddagger$ ) in this reaction (eq 5, where  $k$  is a rate constant,  $T$  is absolute temperature,  $\Delta H^\ddagger$  is enthalpy of activation,  $R$  is the gas

constant (1.987 cal mol<sup>-1</sup> K<sup>-1</sup>),  $k_B$  is the Boltzmann constant (1.381 × 10<sup>-23</sup> J K<sup>-1</sup>),  $h$  is Planck's constant (6.626 × 10<sup>-34</sup> J s), and  $\Delta S^\ddagger$  is the entropy of activation).<sup>51,52</sup> The linear form of the Eyring plot is shown in eq 6. The plot of  $\ln(k/T)$  versus  $1/T$  gives a straight line with a slope of  $-\Delta H^\ddagger/R$  from which the value of the enthalpy of activation can be derived.

$$k = \left( \frac{k_B T}{h} \right) \exp \left( \frac{\Delta S^\ddagger}{R} \right) \exp \left( -\frac{\Delta H^\ddagger}{RT} \right) \quad (5)$$

$$\ln \frac{k}{T} = -\frac{\Delta H^\ddagger}{R} \frac{1}{T} + \ln \frac{k_B}{h} + \frac{\Delta S^\ddagger}{R} \quad (6)$$

**Reaction of Variant P2O with O<sub>2</sub>.** The previous study indicated that the H548A, H548C, H548S, and H548N variant enzymes contained mixed populations of covalently linked and noncovalent flavins.<sup>53</sup> Therefore, in order to investigate the role of His548 in flavin oxidation, double mutations containing both His548 and H167A (a mutation in which the covalent histidyl-FAD linkage was removed) in addition to single mutations were constructed. We have shown previously that the H167A variant enzyme reacts with molecular oxygen to form C4a-hydroperoxyflavin with rate constants similar to those found for the wild-type enzyme, indicating that the covalent linkage is not an important factor for formation of the intermediate.<sup>49</sup> The effects of removal of a covalent histidyl-FAD linkage are mainly on the reductive half-reaction.<sup>49</sup> Therefore, the absence of the covalent histidyl-FAD linkage in P2O variants in this study should not introduce any confounding artifacts to the kinetic analysis.

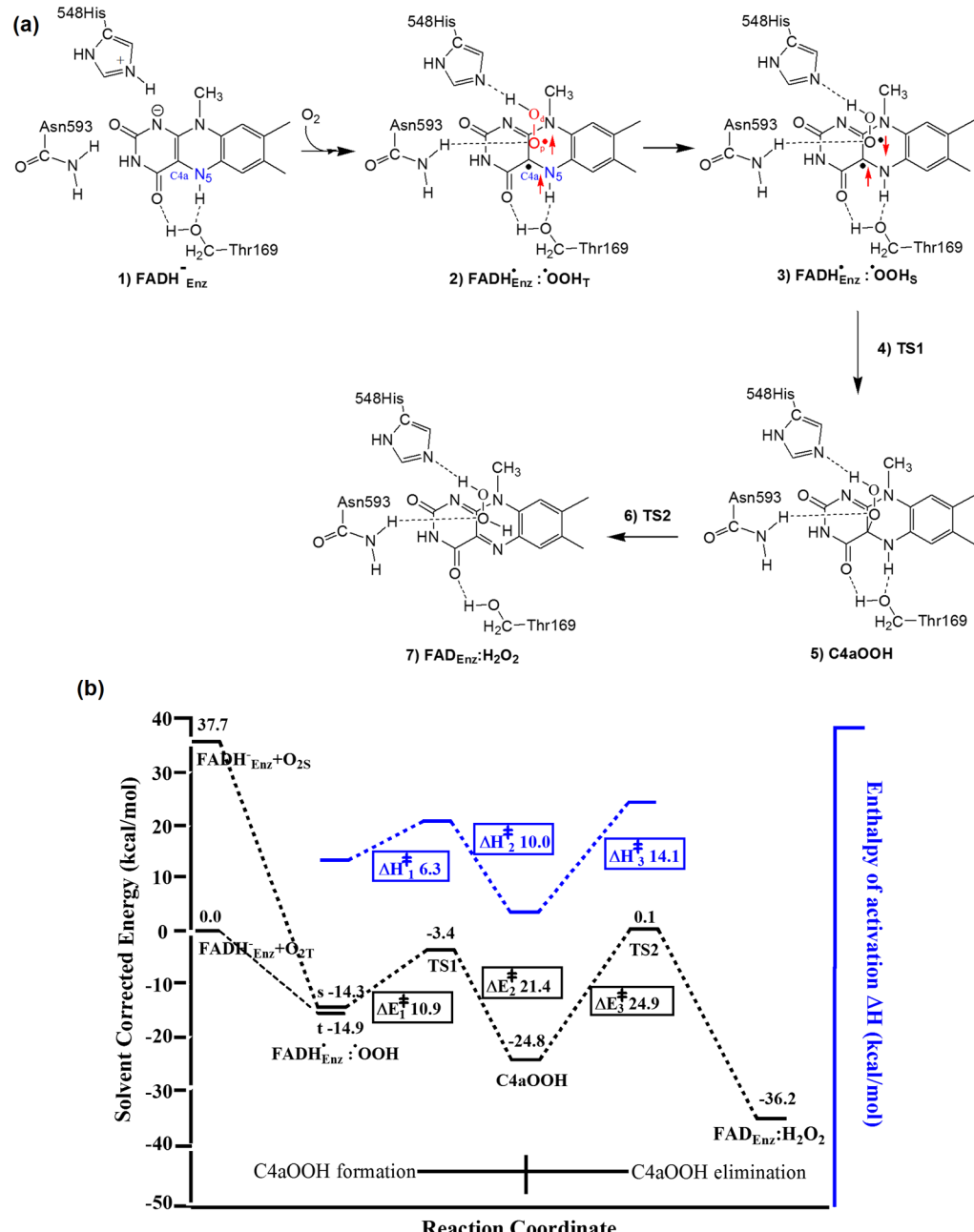
For studying the oxidative half-reaction of N593H and H167A/H548 variant enzymes, an anaerobic enzyme solution was equilibrated in an anaerobic glovebox (as described above). The enzyme was then reduced with a solution of 10 mM D-glucose in 100 mM sodium phosphate buffer pH 7.0 for the N593H variant enzyme. For H167A/H548A, H167A/H548C, H167A/H548S, and H167A/H548N variants which are catalytically inactive for the reductive half-reaction, the enzymes were reduced with a solution of 10 mM sodium dithionite. The oxidation of reduced variant enzyme by O<sub>2</sub> was monitored at various wavelengths (300–500 nm) using a stopped-flow spectrophotometer. Buffer solutions with various concentrations of O<sub>2</sub> were made by bubbling certified O<sub>2</sub>/N<sub>2</sub> gas mixtures of 20%, 50%, 100%, and 100% on ice through syringes for 8 min. After mixing, this procedure resulted in O<sub>2</sub> concentrations of 0.13 mM, 0.31 mM, 0.61 mM, and 0.96 mM, respectively. Equilibration of a buffer on ice with a 100% O<sub>2</sub>/N<sub>2</sub> gas mixture results in a buffer solution that contains 1.92 mM O<sub>2</sub> before mixing. Apparent rate constants ( $k_{\text{obs}}$ ) from kinetic traces were calculated as described above.

**Imidazole Rescue Experiment.** The imidazole rescue experiments on H167A/H548 variants were investigated over a pH range from 6.0 to 8.0 using 100 mM sodium phosphate for pH 6.0 and 7.0, and 100 mM Tris-HCl for pH 8.0. The enzyme solution was mixed with 100 μM imidazole and exchanged into each pH buffer. The resulting solution was equilibrated at that pH for 14–16 h (overnight). Sodium dithionite solutions which were used for reducing the enzyme were prepared by dissolving solid sodium dithionite powder into each pH buffer. A reduced variant enzyme solution was prepared as previously described, and the experiments were done at various pH values. Experimental protocols were similar to those described above.

## RESULTS

**QM Analysis of the Reaction of Reduced P2O with Oxygen (oxidative half-reaction).** The density functional calculations described in Experimental Procedures were used to analyze the physical parameters associated with the individual steps and transition states of the reaction of the P2O-bound FADH<sup>-</sup> (FADH<sup>-</sup><sub>Enz</sub>) (truncated at only the isoalloxazine ring) and dioxygen.

The starting flavin species was assigned as an anionic form in which the N1 position is deprotonated (species 1 in Scheme 3).

Scheme 3. Reaction of P2O-Bound Reduced FAD ( $\text{FADH}^-_{\text{Enz}}$ ) with Oxygen<sup>a</sup>

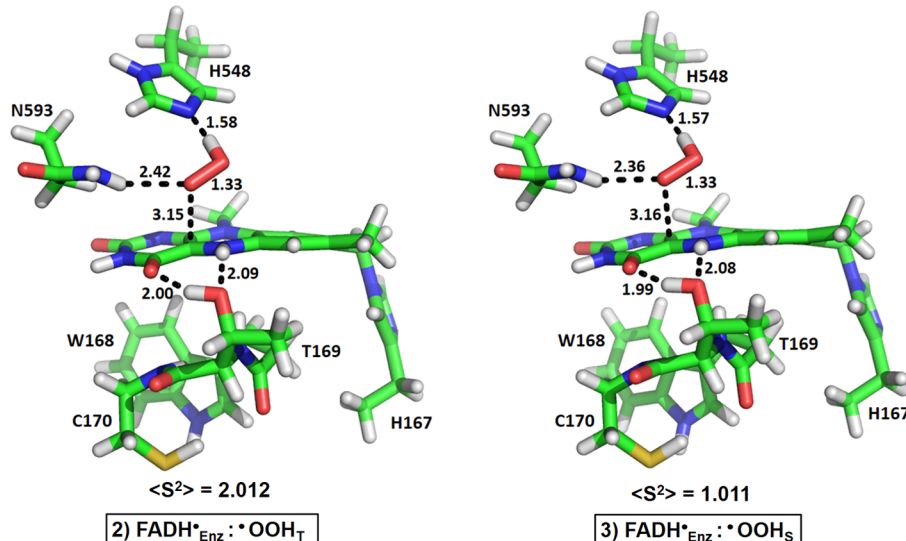
<sup>a</sup>(a) Proposed mechanisms for the reaction of  $\text{FADH}^-_{\text{Enz}}$  with oxygen. Stage 1 is C4a-hydroperoxyflavin formation (1–5) while Stage 2 is  $\text{H}_2\text{O}_2$  elimination and oxidized flavin generation (5–7). (b) Calculated energy profiles along the proposed reaction pathway. The enthalpy of activation obtained from the transient kinetics results in Figure 5 is overlaid in blue.

The relevance of this form in the P2O reaction is supported by the fact that the oxidized enzyme can react with sulfite to form the flavin N(5)-sulfite adduct in which the flavin N1 is in the anionic form.<sup>54</sup> In general, the anionic form of the reduced flavin is the form that is bound to flavoenzyme oxidases.<sup>55</sup> Based on the active site structure of P2O,<sup>45</sup> residues approximately 5 Å away from the N5 atom of the  $\text{FADH}^-$  (Trp168, Thr169, and Cys170) and the key conserved residues (His167, His548, and Asn593) were included in the QM model (Figure 1).

Among these residues, His548 is the most likely to be in the protonated state. According to previous studies of P2O, upon completion of the reductive half-reaction, the oxidized flavin is

reduced by D-glucose, and His548 is expected to be in the protonated state.<sup>53</sup> Furthermore, the results of pH-dependence studies of the oxidative half-reaction at various pH values suggest that one of the active site residues should be protonated to allow the reaction to proceed via formation of C4a-hydroperoxyflavin.<sup>50</sup> On the basis of these findings, the calculation model was started with His548 in the protonated state (species 1 in Scheme 3).

Transient kinetics studies of the P2O oxidative half-reaction indicated that the reaction proceeds via two stages, involving C4a-hydroperoxyflavin formation and decay ( $\text{H}_2\text{O}_2$  elimination).<sup>18,50,56</sup> Results from the density functional calculations give insights into the electronic structures, spin states, and



	$\text{FADH}^{\cdot}\text{Enz} : \cdot\text{OOH}_T$	$\text{FADH}^{\cdot}\text{Enz} : \cdot\text{OOH}_S$	$\text{FADH}^{\cdot}\text{Free} : \cdot\text{OOH}_T$	$\text{FADH}^{\cdot}\text{Free} : \cdot\text{OOH}_S$	$\text{FADH}^{-}\text{Free} : \text{O}_{2T}$	$\text{FADH}^{-}\text{Free} : \text{O}_{2S}$	$\text{O}_{2T}$	$\text{O}_{2S}$
$\Delta E_{S-T}$ (kcal/mol)	0.6		0.0		7.3		37.7	
$q_{O-O}$	-0.480	-0.469	-0.424	-0.423	-0.249	-0.273	0.000	0.000
$q_{OOH}$	-0.081	-0.080	-0.028	-0.028	-	-	-	-
$\rho_{O-O}$	+1.013	-1.011	+1.017	+1.019	+1.702	+0.007	+2.000	0.000
$\rho_{OOH}$	+1.004	-1.002	+1.007	+1.010	-	-	-	-
$\rho_{\text{Flavin}}$	+0.991	+0.990	+1.015	-1.010	+0.304	-0.005	-	-
$d_{O_p-O_d} (\text{\AA})$	1.33	1.33	1.32	1.32	1.25	1.25	1.21	1.21

**Figure 2.** Optimized structures of  $\text{FADH}^{\cdot}\text{Enz} : \cdot\text{OOH}$  complexes. The subscripts T and S represent triplet state and singlet state, respectively.  $\Delta E_{S-T}$  represents the energy difference between the spin-unrestricted open-shell singlet state and the triplet state. Mulliken charge populations ( $q$ ) on the two oxygen atoms ( $q_{O-O}$ ) of the  $\cdot\text{OOH}$  fragment and on the  $\cdot\text{OOH}$  fragment ( $q_{OOH}$ ) are shown. Mulliken spin populations ( $\rho$ ) on the  $\text{O}_2$  ( $\rho_{O-O}$ ),  $\cdot\text{OOH}$  ( $\rho_{OOH}$ ), and flavin ( $\rho_{\text{Flavin}}$ ) fragments are shown. Distances between the two oxygen atoms on the  $\cdot\text{OOH}$  fragment ( $d_{O_p-O_d}$ ) are shown in Å.

energies of the transition states and intermediates involved (Figure 2–4), and point to a five-step process (Scheme 3).

**Step 1: Proton-Coupled Electron Transfer to Triplet Dioxygen (Species 1 to Species 2).** The energy of the first species,  $\text{FADH}^{\cdot}\text{Enz} + \text{O}_{2T}$  (or  $\text{FADH}^{\cdot}\text{Enz} + \text{O}_{2S}$ ), is a combination of the electronic energy with solvation correction from the optimized structure of  $\text{FADH}^{\cdot}\text{Enz}$  (species 1) and that of  $\text{O}_{2T}$  (or  $\text{O}_{2S}$ ). The stabilized complex of reduced flavin ( $\text{FADH}^{\cdot}\text{Enz}$ ) and dioxygen was found to be improbable through calculations. After several attempts, when the  $\text{O}_2$  was placed in the vicinity above the C4a position and upon geometry optimization, the proton from the protonated His548 was immediately transferred to the dioxygen. This was concomitant with the first electron transfer from the reduced flavin to the dioxygen to generate the flavin semiquinone: $\cdot\text{OOH}$  radical pair in the triplet state ( $\text{FADH}^{\cdot}\text{Enz} : \cdot\text{OOH}_T$ ) (Figure 2). It should be mentioned that when this reaction step was calculated using other functionals such as TPSS, the concomitant proton and electron transfer was similar to the results obtained using B3LYP.

Mulliken charge populations on the two oxygen atoms of the  $\text{FADH}^{\cdot}\text{Enz} : \cdot\text{OOH}_T$  ( $-0.480$ ) are relatively more negative than that of the triplet dioxygen ( $0.000$ ); this indicates that an electron is transferred to  $\cdot\text{OOH}$ . As the charge population on the overall  $\cdot\text{OOH}$  fragment is  $-0.081$ , the concomitant electron and proton transfer neutralizes the negative charge of the

superoxide species and increases the ability of dioxygen to accept an electron from  $\text{FADH}^{\cdot}\text{Enz}$ . Mulliken spin populations on the  $\text{OOH}$  ( $+1.004$ ) and the flavin ( $+0.991$ ) fragments reveal the identity of species 2 as the triplet  $\text{FADH}^{\cdot}\text{Enz} : \cdot\text{OOH}_T$  (Table in Figure 2), with a single unpaired electron located on each of the OOH and the flavin fragments.

Note that the proton-coupled electron transfer process for the reaction of reduced flavin and dioxygen presented here is different from the current view<sup>7,9</sup> that describes the first step as an electron transfer to generate a radical pair of flavinsemiquinone and superoxide anion before the subsequent proton transfer occurs (paths a and b in Scheme 1).

**Step 2: Triplet ( $\text{FADH}^{\cdot}\text{Enz} : \cdot\text{OOH}_T$ ) to singlet ( $\text{FADH}^{\cdot}\text{Enz} : \cdot\text{OOH}_S$ ) Spin Transition (Species 2 to Species 3).** The triplet ( $\text{FADH}^{\cdot}\text{Enz} : \cdot\text{OOH}_T$ ) can undergo a spin transition with a small energy requirement ( $+0.6$  kcal/mol, Scheme 3, Table in Figure 2) to become an open-shell singlet diradical ( $\text{FADH}^{\cdot}\text{Enz} : \cdot\text{OOH}_S$ ), in which the spin populations on the OOH fragment change from  $+1.004$  to  $-1.002$ , but remain the same on the flavin fragment at about  $+0.99$  (Table in Figure 2, Figure S3 in SI). Overall, the structural geometries of the triplet  $\text{FADH}^{\cdot}\text{Enz} : \cdot\text{OOH}_T$  and the open-shell singlet diradical  $\text{FADH}^{\cdot}\text{Enz} : \cdot\text{OOH}_S$  complexes are similar (Table in Figure 2). The  $\text{O}_p - \text{O}_d$  bond distance in both  $\text{FADH}^{\cdot}\text{Enz} : \cdot\text{OOH}_T$  and  $\text{FADH}^{\cdot}\text{Enz} : \cdot\text{OOH}_S$  ( $1.33$  Å) is significantly longer than that in the  $\text{O}_{2T}$  ( $1.21$  Å),

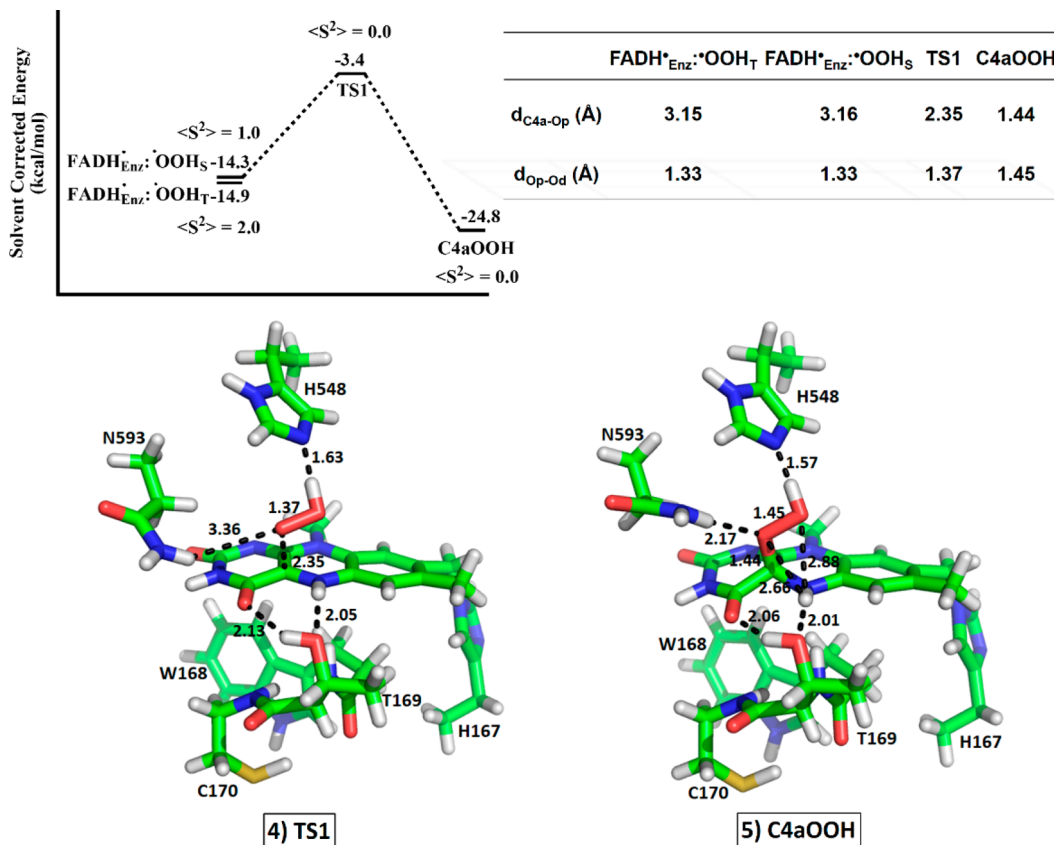


**Figure 3.** Relative energy profiles for the formation of C4a-hydroperoxyflavin intermediate (C4aOOH, species 5 in Scheme 3). The optimized structures of transition state 1 (TS1) and the C4aOOH intermediate are shown. The C4a–O<sub>p</sub> distance ( $d_{C4a-Op}$ ) and the O<sub>p</sub>–O<sub>d</sub> distance ( $d_{Op-Od}$ ) are shown in the table.

corresponding to the addition of one electron into the antibonding orbital of the dioxygen.

To identify the active site residues involved in the P2O dioxygen activation process, we studied this process in the absence of all residues. Thus, the electronic structures and energies in both triplet and open-shell singlet states for the dioxygen (O<sub>2</sub>), the FADH<sub>Free</sub>:O<sub>2</sub> complex, and the FADH<sub>Free</sub>:OOH complex were investigated in order to compare them with those for the FADH<sup>+</sup><sub>Enz</sub>:OOH. For dioxygen (O<sub>2</sub>) in the absence of a flavin cofactor, the spin transition process from the triplet O<sub>2T</sub> ( $\rho_{O-O} = +2.000$ ) to the singlet O<sub>2S</sub> ( $\rho_{O-O} = 0.000$ ) requires a large energy input of 37.7 kcal/mol (Table in Figure 2). The O<sub>p</sub>–O<sub>d</sub> bond distances in both spin states are similar (1.21 Å) (Table in Figure 2).

To explore the effects of a flavin cofactor, the FADH<sub>Free</sub>:O<sub>2</sub> model was investigated (Figure S1, SI). The spin transition proceeding from the triplet FADH<sub>Free</sub>:O<sub>2T</sub> to the open-shell singlet FADH<sub>Free</sub>:O<sub>2S</sub> requires 7.3 kcal/mol of energy, which is significantly lower than that of the dioxygen (37.7 kcal/mol) (Table in Figure 2). The spin population on the O<sub>2</sub> fragment (+1.702) of the triplet FADH<sub>Free</sub>:O<sub>2T</sub> (Table in Figure 2 and Figure S1, SI) is slightly less than that on the free triplet O<sub>2T</sub> (+2.000). The charge population on the dioxygen fragment is -0.249, and the O<sub>p</sub>–O<sub>d</sub> bond becomes slightly weaker (1.25 Å) than that found in the free triplet O<sub>2T</sub> (1.21 Å). These findings imply that the presence of a flavin cofactor causes some charge transfer to the dioxygen, which also results in a decrease in the energy gap between the singlet and the triplet states. The C<sub>4a</sub>–O<sub>p</sub> distance is shorter in the open-shell singlet FADH<sub>Free</sub>:O<sub>2S</sub> (3.10 Å) complex when compared with that

of the triplet FADH<sub>Free</sub>:O<sub>2T</sub> (3.23 Å) complex (Table S3, SI). Altogether, our data indicate that the flavin cofactor partly assists with the electron transfer and spin transition process.

To evaluate the importance of protonation in the dioxygen activation process, an additional proton was included into the triplet FADH<sub>Free</sub>:O<sub>2T</sub> and the open-shell singlet FADH<sub>Free</sub>:O<sub>2S</sub> models giving the triplet FADH<sub>Free</sub>:OOH<sub>T</sub> and the open-shell singlet FADH<sub>Free</sub>:OOH<sub>S</sub>, respectively (Figure S2, SI). Interestingly, with an additional proton, the energy difference between the FADH<sub>Free</sub>:OOH<sub>T</sub> and the FADH<sub>Free</sub>:OOH<sub>S</sub> complexes became insignificant (0.01 kcal/mol) (Table in Figure 2). Unlike the triplet FADH<sub>Free</sub>:O<sub>2T</sub>, in which only partial charge is transferred from the flavin to the dioxygen, the electronic structure of the triplet FADH<sub>Free</sub>:OOH<sub>T</sub> implies that one electron is transferred from the flavin to the OOH fragment; the FADH<sub>Free</sub>:OOH<sub>T</sub> complex contains similar spin populations on the OOH (+1.007) and the flavin (+1.015) fragments. The O<sub>p</sub>–O<sub>d</sub> bond distance in the FADH<sub>Free</sub>:OOH<sub>T</sub> (1.32 Å) complex is also weaker than that found in the FADH<sub>Free</sub>:O<sub>2T</sub> complex (1.25 Å) (Table in Figure 2).

The open-shell singlet FADH<sub>Free</sub>:OOH<sub>S</sub> complex was identified as the open-shell singlet diradical species with a spin population on the OOH fragment of +1.010 and on the flavin fragment of -1.010 (Table in Figure 2, Figure S2, SI). The structural geometries of the triplet FADH<sub>Free</sub>:OOH<sub>T</sub> and the open-shell singlet diradical FADH<sub>Free</sub>:OOH<sub>S</sub> complexes are similar; the C<sub>4a</sub>–O<sub>p</sub> distances of both spin states are about the same (3.75 Å) (Table S3, SI). Altogether, the data indicate that the additional proton facilitates the spin transition, as the energy required for this process is reduced.

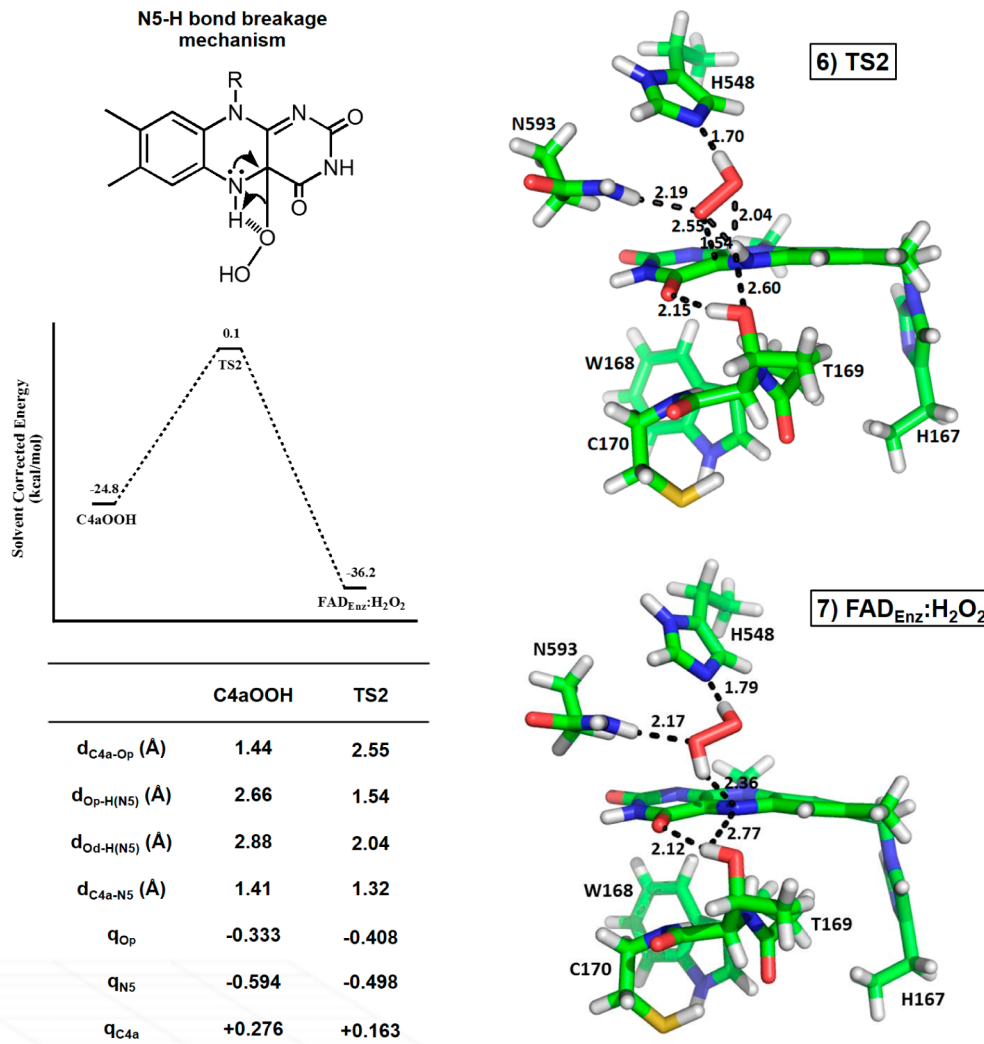


**Figure 4.** Relative energy profiles of H<sub>2</sub>O<sub>2</sub> elimination from C4a-hydroperoxyflavin, the optimized structures of TS2, and the final product FAD<sub>Enz</sub>:H<sub>2</sub>O<sub>2</sub> complex. Values for the C4a–O<sub>p</sub> distance ( $d_{C4a-O_p}$ ), O<sub>p</sub>–H(N5) distance ( $d_{O_p-H(N5)}$ ), O<sub>d</sub>–H(N5) distance ( $d_{O_d-H(N5)}$ ), and C4a–N5 distance ( $d_{C4a-N5}$ ) are shown in the table. Mulliken charge populations on the O<sub>p</sub> ( $q_{O_p}$ ), the N5 ( $q_{N5}$ ), and the C4a ( $q_{C4a}$ ) are also shown.

This result highlights the importance of the proton-coupled electron transfer process as a driving factor that facilitates the formation of the open-shell singlet diradical species (FADH·<sub>Free</sub>·OOH<sub>S</sub>). In P2O, the protonated His548 plays an important role in the supply of a proton to the dioxygen during the first electron transfer process to mediate the formation of FADH·<sub>Enz</sub>·OOH<sub>S</sub>.

**Step 3: C4a-Hydroperoxyflavin Formation and TS1 (Species 3 to Species 5).** In the open-shell singlet diradical FADH·<sub>Enz</sub>·OOH<sub>S</sub> complex, the opposite spins on the ·OOH (−1.002) and the flavin (+0.990) fragments facilitate bond formation between the proximal oxygen (O<sub>p</sub>) of ·OOH and the C4a of the isoalloxazine ring (Figure 2) to form the C4aOOH via TS1 (Figure 3). Two hydrogen-bond interactions from the N<sup>ε</sup> of His548 (1.57 Å) and the N<sup>δ</sup>H of Asn593 (2.36 Å) to the ·OOH fragment (Figure 2) play a role in positioning the O<sub>p</sub> atom of the ·OOH fragment; the O<sub>p</sub> is located directly above the flavin C4a position. In FADH·<sub>Enz</sub>·OOH<sub>S</sub>, the C4a–O<sub>p</sub> distance is 3.16 Å and the O<sub>p</sub>–O<sub>d</sub> distance is 1.33 Å (Figure 2, Table in Figure 3). In TS1, the C4a–O<sub>p</sub> distance is shortened to 2.35 Å and the O<sub>p</sub>–O<sub>d</sub> distance is lengthened to 1.37 Å. The activation energy for this step is 10.9 kcal/mol. Once TS1 transforms to the C4aOOH, the C4a–O<sub>p</sub> bond is completely

formed (1.44 Å) and the O<sub>p</sub>–O<sub>d</sub> bond distance has a single bond character (1.45 Å) (calculated O–O bond distance in H<sub>2</sub>O<sub>2</sub> is 1.46 Å) (Table in Figure 3).

The position of the –OOH moiety of the C4aOOH intermediate above the flavin ring is consistent with the conventional assignment of being *re*-side and compatible with a “face-on” configuration (Figure 3). As most flavoenzymes that form C4aOOH only have space available on the *re*-side to accommodate the –OOH moiety, we explored the P2O preference for C4aOOH formation on the *re*-side versus the *si*-side.

In the absence of the active site residues of P2O, we calculated the energy of H<sub>2</sub>O<sub>2</sub> elimination from the C4aOOH intermediate for the free flavin model, where the –OOH moiety is located above (*re*-side) and below (*si*-side) the C4a position of the isoalloxazine ring (Figure S4, SI). The reaction on both sides of the ring essentially required the same amount of energy (29.7 kcal/mol). Thus, the preference for the *re*-side reaction in P2O (and other flavoenzymes) is not attributed to the differences in the electronic effect above and below the isoalloxazine ring.

In the P2O active site, the *si*-side of the isoalloxazine ring is, in fact, crowded with bulky active site residues (Trp168 and

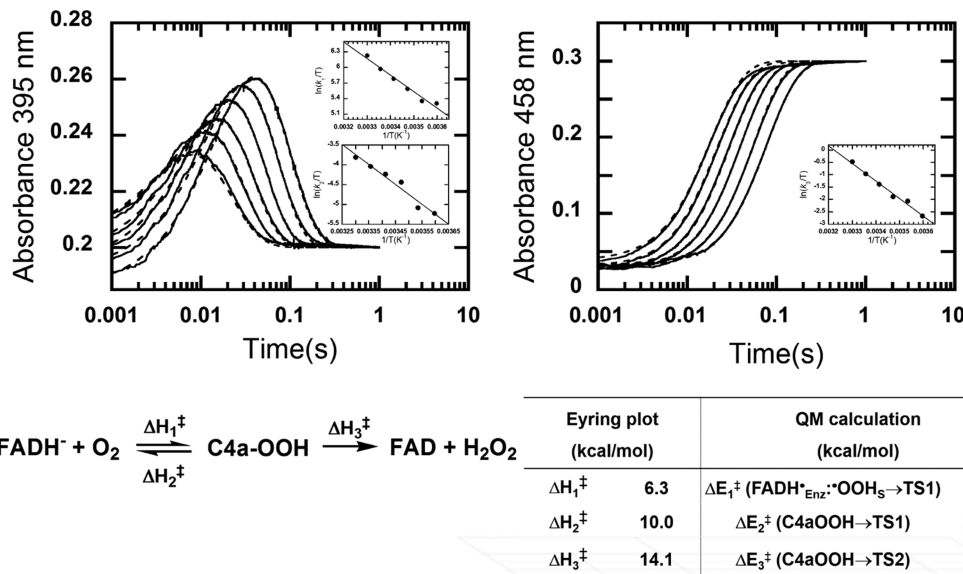


**Figure 5.** Oxidative half-reaction of P2O at various temperatures and Eyring plots. The transient kinetics of the oxidative half-reaction of P2O was investigated at various temperatures (5, 10, 15, 20, 25, and 30 °C) using stopped-flow spectrophotometry. Kinetic simulations with a two-step consecutive model (dotted line traces) according to the method described in ref 18 were used for analysis of rate constants. Insets show the Eyring plots of rate constants for formation ( $k_1$ ), decay of C4a–OOH ( $k_2$ ), and H<sub>2</sub>O<sub>2</sub> elimination ( $k_3$ ). The enthalpy of activation from the Eyring plots and the activation energies from QM calculations are summarized in the table, and the values were also plotted in Scheme 3

Cys170), while the *re*-side has an empty cavity for accommodating O<sub>2</sub> and the resulting –OOH moiety. Therefore, the preference for the *re*-side reaction in P2O is mainly due to the steric hindrance effects on the *si*-side. Trp168 and Cys170 are thus important for directing the formation of the C4aOOH on the *re*-side in P2O.

**Steps 4 and 5: H<sub>2</sub>O<sub>2</sub> Elimination from C4a-Hydroperoxyflavin and TS2 (Species 5 to Species 7).** There are four hydrogen-bond interactions to the –OOH moiety and the isoalloxazine ring of the C4aOOH intermediate: (1) the N<sup>ε</sup> of His548 accepts a hydrogen bond from the –OOH moiety (1.57 Å), (2) the N<sup>δ</sup>H of Asn593 donates a hydrogen bond to the O<sub>p</sub> of OOH moiety (2.17 Å), (3) the O<sup>γ</sup> of Thr169 accepts a hydrogen bond from the NSH of the isoalloxazine (2.01 Å), and (4) the –O<sup>γ</sup>H of Thr169 donates a hydrogen bond to the O<sub>4</sub> of the isoalloxazine (2.06 Å) (Figure 3). Among these hydrogen bonds, the one from Asn593 in the C4aOOH intermediate (species 5) is significantly stronger (2.17 Å) than the corresponding one in species 2–4 (>2.36 Å). Thus, Asn593 is not only positioning the O<sub>p</sub> atom of the ·OOH to be directly above the flavin C4a position to form the C4aOOH intermediate, it is also stabilizing the C4aOOH intermediate by tightening the hydrogen-bond interaction.

For H<sub>2</sub>O<sub>2</sub> elimination, a direct proton transfer from the flavin N5–H to the O<sub>p</sub> of a peroxide leaving group can occur with a calculated activation energy (from C4aOOH to TS2) of 24.9 kcal/mol (Figure 4), making it the rate-limiting step in the oxidative half-reaction of P2O. The C4aOOH has a C4a–O<sub>p</sub> distance of 1.44 Å and an O<sub>p</sub>–H(N5) distance of 2.66 Å (Figure 3, Table in Figure 4). In TS2, the C4a–O<sub>p</sub> distance is lengthened to 2.55 Å and the O<sub>p</sub>–H(NS) distance is shortened to 1.54 Å. As the O<sub>d</sub>–H(NS) distance is also shortened from 2.88 Å in C4a–OOH to 2.04 Å in TS2, the proton transfer from N5 to O<sub>p</sub> of a peroxide leaving group is mediated through the N5 and O<sub>d</sub> interaction.

The bond distance between the O<sup>γ</sup> of Thr169 and the NSH of the isoalloxazine in TS2 (2.60 Å) is relatively weaker than

that found in C4aOOH (2.01 Å). Thus, the hydrogen bonds from Thr169 appear to be flexible, i.e. changing from a tight interaction which stabilizes C4aOOH to a more relaxed interaction in the H<sub>2</sub>O<sub>2</sub> elimination process. The loosening of the hydrogen-bond interaction between O<sup>γ</sup> of Thr169 and the NSH of the isoalloxazine in TS2 is also consistent with experimental observation. Variants of Thr169, in which the interaction at the flavin NSH is absent, do not stabilize the C4aOOH intermediate.<sup>48</sup>

The intramolecular proton transfer step to eliminate H<sub>2</sub>O<sub>2</sub> via TS2 is consistent with previous experimental data showing that H<sub>2</sub>O<sub>2</sub> elimination from the C4aOOH intermediate is controlled by a single proton transfer from the flavin N5 to an O<sub>p</sub> of a peroxide leaving group.<sup>56</sup> Stopped-flow experiments showed that mutation of His548, Asn593 (see results in Figure 6 and Figures S6–S8 in SI), and Thr169<sup>48</sup> resulted in abolishing C4a-hydroperoxyflavin formation. This is consistent with our calculations that reveal the importance of protonated His548 for proton-coupled electron transfer to activate dioxygen to form the C4aOOH intermediate and the role of hydrogen bonds from Asn593, His548 and Thr169 in stabilizing the C4aOOH intermediate.

Once the proton is transferred from the flavin N5 to a peroxide leaving group to form the FAD<sub>Enz</sub>:H<sub>2</sub>O<sub>2</sub> complex (species 7), the C4a–O<sub>p</sub> distance is lengthened to 3.27 Å, confirming cleavage of the C4a–O<sub>p</sub> bond. Overall, the process of H<sub>2</sub>O<sub>2</sub> elimination results in a release of energy of -36.2 kcal/mol. The reverse reaction via TS2 needs to overcome an energy barrier of +36.3 kcal/mol. Thus, formation of H<sub>2</sub>O<sub>2</sub> tends to be irreversible, and H<sub>2</sub>O<sub>2</sub> departure from the active site is presumably facilitated by conformational changes of the P2O enzyme.<sup>45,57</sup>

**Activation Energy of the Reaction of Reduced P2O with Oxygen Analyzed by the Eyring Equation.** To complement our density functional calculations, reactions of reduced P2O with dioxygen at various temperatures (5–30 °C) were carried out using stopped-flow spectrophotometry to

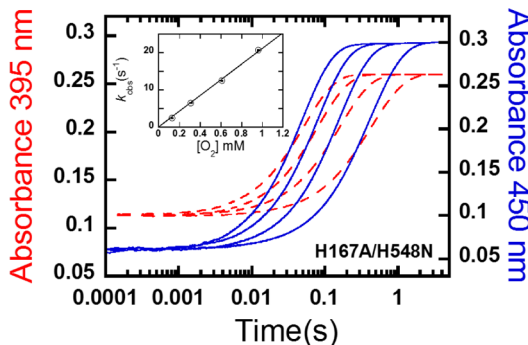


**Figure 6.** Kinetics of the reactions of reduced H167A/H548N variant with O<sub>2</sub>. The data show monophasic kinetics, indicating that flavin is oxidized without forming C4a-hydroperoxyflavin. The inset shows the observed rate constants which are linearly dependent on O<sub>2</sub> concentrations. Summary of bimolecular rate constants of the oxidative half-reactions of N593H and H167A/H548 variants are shown in the table.

determine the enthalpy of activation ( $\Delta H^\ddagger$ ) for C4aOOH formation from the reaction of FADH<sup>-</sup><sub>Enz</sub> and O<sub>2</sub> in both forward and reverse directions, and for H<sub>2</sub>O<sub>2</sub> elimination (Experimental Procedures). As determined by analysis of the Eyring plot, the transient kinetics data (Figure 5, Table S4 and Figure S5) show that the enthalpy of activation for C4aOOH formation from the reaction of FADH<sup>-</sup><sub>Enz</sub> and O<sub>2</sub> in the forward direction ( $\Delta H_1^\ddagger$ ) is 6.3 kcal/mol and in the reverse reaction ( $\Delta H_2^\ddagger$ ) is 10.0 kcal/mol. The enthalpy for H<sub>2</sub>O<sub>2</sub> elimination ( $\Delta H_3^\ddagger$ ) is 14.1 kcal/mol. The calculated energy barrier is in agreement with the experimental enthalpy barrier in that the energy barrier for C4aOOH formation is lower than that for its reverse reaction ( $\Delta E_1^\ddagger$  and  $\Delta E_2^\ddagger$  vs  $\Delta H_1^\ddagger$  and  $\Delta H_2^\ddagger$ ) (Scheme 3, table in Figure 5). Proton abstraction from NSH was determined as the rate-determining step as the energy barrier for H<sub>2</sub>O<sub>2</sub> elimination is the highest ( $\Delta E_3^\ddagger$  and  $\Delta H_3^\ddagger$ ). Since only the active site as a part of the enzyme was considered in the model studied for computational feasibility and the corrections for zero-point vibrational energy and thermal effects cannot be included in the calculation, we expect some discrepancies between the calculated energy and the experimental enthalpy to exist. A similar level of discrepancy between experimental and calculation results was also present in other works.<sup>58</sup> Overall, the results show that the relative activation energy ( $\Delta E^\ddagger$ ) displays the same trend as the relative enthalpy of activation ( $\Delta H^\ddagger$ ) derived experimentally from the Eyring plots. Specifically, this implies that the energy change for O<sub>2</sub> activation by P2O mainly derives from the change of electronic structures of the intermediates and transition states involved.

**Transient Kinetics of Reactions of Reduced H548 and N593 Variants with Oxygen.** Transient kinetic experiments for Asn593 variant (N593H), and His548 variants (H167A/H548A, H167A/H548C, H167A/H548S, and H167A/H548N) were performed to confirm the involvement of these two conserved residues in stabilization of C4a-hydroperoxyflavin. For the oxidative half-reactions of P2O(WT) and H167A variant enzymes,<sup>18,49</sup> the reaction shows biphasic kinetics, indicating formation of a C4a-hydroperoxyflavin intermediate (Figure 5). For His548 and Asn593 variants, the results showed only one kinetic phase, indicating that only flavin oxidation was observed (Figure 6 and Figures S6–S8 in SI). These data indicate that a C4a-hydroperoxyflavin intermediate does not form in these variants (Figure 6, Figures S6–S8 in SI), confirming the findings from QM calculations that His548 and Asn593 are important for stabilization of C4a-hydroperoxy-

Variants	Bimolecular rate constant (M <sup>-1</sup> s <sup>-1</sup> )
H167A/H548A	58 ± 2
H167A/H548C	233 ± 3
H167A/H548S	359 ± 2
H167A/H548N	21,000 ± 8
N593H	529 ± 6

flavin. Moreover, when the imidazole rescue experiment for His548 variants at various pHs was performed, the results were similar to those in the absence of imidazole in which no C4a-hydroperoxyflavin was detected (Table S5, SI). These results indicate that not only is a proton required, but proper geometry of the protonated His548 in the active site of the P2O enzyme is mandatory for formation of the C4a-hydroperoxyflavin intermediate.

Our previously published results for T169A, T169S, T169N, and T169G variants indicated that all of these variants also void formation of C4a-hydroperoxyflavin.<sup>48</sup> Therefore, the QM analysis results in which Thr169, His548, and Asn593 were identified as residues important for the stabilization of TS1 and C4a-hydroperoxyflavin are supported well by stopped-flow studies of the variant enzymes.

## DISCUSSION

Our findings based on QM analysis and transient kinetic studies have identified the physical factors underlying the reaction of reduced flavin and dioxygen catalyzed by P2O. The data provide mechanistic insight that is different from the general model currently used for explaining the reaction of reduced flavin and oxygen.<sup>6,9,55</sup> The initial protonation of dioxygen by His548 of P2O that occurs in a concerted manner with an electron transfer is key for the oxygen activation process. The data obtained from QM analysis and transient kinetics indicate that the –OOH moiety of the C4a-hydroperoxyflavin is stabilized via a “face-on” configuration. The C4a-hydroperoxyflavin is stabilized by the hydrogen-bond interactions from His548, Asn593, and Thr169. H<sub>2</sub>O<sub>2</sub> elimination occurs via a direct proton transfer from the flavin N5–H. The trends observed for the energy profiles based on the QM results also correlated well with the enthalpy of activation profiles obtained from the Eyring plots.

The data in Figure 2 suggest that the first step of the P2O reaction is a single electron transfer that is coupled with a proton transfer. The relative timing of proton transfer in Figure 2 is different from the current views toward the reaction of reduced flavin and oxygen in flavoenzymes which propose that a single electron is first transferred to form the flavin semiquinone and superoxide radical pair (paths a and b in Scheme 1<sup>6,7,9</sup>). A new model based on our results can be summarized as in Scheme 1, path C. Results from DFT calculations agree well with the experimental data because they suggest that no net proton transfer is involved in the TS1 transformation to the C4a-hydroperoxyflavin intermediate

(Figure 3), which is consistent with the previous experiments indicating that no solvent kinetic isotope effect (SKIE) was detected for the C4a-hydroperoxyflavin formation.<sup>56</sup> However, with a similar calculation method, different results were obtained for the QM analysis of flavindestuctase (BluB) because the first step of the BluB-catalyzed reaction is a single electron transfer from reduced flavin to dioxygen to generate the flavin semiquinone and superoxide radical pair before it collapses to form a negatively charged C4a-flavin peroxide intermediate. This intermediate is stabilized by two hydrogen bonds from the backbone amide of Gly61 and the O<sub>2</sub> hydroxyl group of reduced FMN.<sup>29</sup> As the next step of BluB reaction is a cleavage of the isoalloxazine ring, it can thus be seen that protonation is not necessary for C4a-flavin peroxide in BluB catalysis. Therefore, different active site environments can influence the relative timing of electron and proton transfers differently.

The DFT analysis and transient kinetics indicate that the conserved His548 in P2O provides an internal proton for oxygen activation. This protonation process makes oxygen a better electron acceptor as the Mulliken charge of dioxygen atoms on the ·OOH molecule in the active site model (−0.480) is more negative than in the free flavin model (−0.249)—the model that describes the unprotonated His548 condition (Figure 2). The His548 and Asn593 help in aligning a ·OOH radical such that it is properly oriented for the next step in C4a-hydroperoxyflavin formation. The DFT results agree well with the experimental data because the reaction at lower pH is much faster than that at higher pH and formation of C4a-hydroperoxyflavin can only be detected at pH values lower than 8.0.<sup>50</sup> Moreover, results from studies of the reductive half-reaction of P2O indicate that the conserved His548, which acts as a general base during the reductive half-reaction, likely exists in the protonated form at the initial stage of the oxidative half-reaction.<sup>53</sup> Therefore, the functional role of His548 in P2O can be viewed as that of a general base in the reductive half-reaction and a general acid in the oxidative half-reaction (path c in Scheme 1).

In addition to P2O, many studies of other flavoenzyme oxidases have shown that positive charges near the flavin N5 are important for the oxygen activation process. For glucose oxidase, the protonated His516 is required because the pH-rate profiles showed that the  $k_{\text{cat}}/K_m(\text{O}_2)$  is 2600-fold higher at lower pH than at higher pH.<sup>59,60</sup> In contrast, for choline oxidase, oxygen activation is thought to be caused by the positive charge of the substrate.<sup>16</sup> For monomeric sarcosine oxidase, N-methyltryptophan oxidase, and fructosamine oxidase, mutation of Lys 256 to a neutral amino acid results in a 550–9000-fold decrease in oxygen reactivity.<sup>13–15</sup> More moderate effects were observed for similar mutations in polyamine oxidase and dihydroorotate dehydrogenase.<sup>15,17</sup> In most of these studies, the role of the positively charged residues was proposed to provide electrostatic interactions to stabilize the formation of a negatively charged superoxide radical. Our current findings suggest that quantum mechanical calculations for these enzymes should be useful for analyzing whether these positively charged residues can act as proton donors similar to what is observed in the P2O reaction.

The DFT optimized structure of C4a-hydroperoxyflavin (Figure 3) offers a molecular view of the physical and chemical interactions required for stabilization of the intermediate in a flavoenzyme. The data show that the intermediate is closely interacting with the side chains of Thr169, His548, and Asn593.

Experimental evidence also confirms that these interactions are important because mutation of His548, Asn593 (Figure 6, Figures S6–S8 in SI), and Thr169 variants<sup>48</sup> failed to stabilize the C4a-hydroperoxyflavin intermediate. Moreover, the imidazole rescue experiment for the His548 variants could not restore the formation of C4a-hydroperoxyflavin (Table S5, SI), implying that the geometry of the general acid (His548) in relation to the flavin position is very important for stabilization of TS1 or C4a-hydroperoxyflavin. It is interesting to note that the ·OOH moiety in Figure 3 is configured in a “face-on” configuration. In most of the X-ray structures of enzymes that can form C4a-hydroperoxyflavin, a cavity above the *re*-face of the flavin C4a atom is common.<sup>6</sup> Therefore, the “face-on” configuration can fit in active sites and may be prevalent in many enzymes.

Data in Figure 4 also confirm that the C4a-hydroperoxyflavin can undergo a unimolecular reaction to generate H<sub>2</sub>O<sub>2</sub>, and the relaxed H-bond interaction between the O<sub>γ</sub> of Thr169 and the N5H of the isoalloxazine in TS2 (bond length of 2.60 Å) could be a key feature that enables this process. In previous studies, when the reduced enzyme which was specifically labeled with a single deuterium atom to give flavin N5-D reacted with dioxygen, a KIE of ~3 for the H<sub>2</sub>O<sub>2</sub> elimination was observed. The KIE is the same as that observed when the reaction was carried out in D<sub>2</sub>O.<sup>56</sup> These experimental results agree well with the formation of species 5, TS2, and species 7. They also provide evidence supporting a unimolecular mechanism of H<sub>2</sub>O<sub>2</sub> elimination consisting of a single proton transfer from N5-H to a peroxide leaving group. The importance of H-bond interactions at the flavin N5 in stabilization of the C4a-hydroperoxyflavin has been observed in many systems. For Thr169 variants of P2O in which a H-bond interaction at the flavin N5 is absent, the C4a-hydroperoxyflavin intermediate could not be detected.<sup>48</sup> In the oxygenase component of *p*-hydroxyphenylacetate hydroxylase, upon removal of the residue (Ser171) that forms hydrogen bonds with the flavin N5, the rate of H<sub>2</sub>O<sub>2</sub> elimination increased by ~1400-fold.<sup>61</sup> For a Baeyer–Villiger monooxygenase, the interaction between the flavin N5 and a bound NADP<sup>+</sup> is necessary in order to stabilize the C4a-hydroperoxyflavin.<sup>62</sup> A recent DFT calculation by Bach and Mattevi<sup>32</sup> suggests that in the absence of protein environment, the H<sub>2</sub>O<sub>2</sub> elimination from C4a-hydroperoxyflavin is not feasible. When H<sub>2</sub>O or CH<sub>3</sub>OH (to model Thr or Ser) was included to serve as a proton shuttle path, the energy barrier for H<sub>2</sub>O<sub>2</sub> elimination significantly decreased. Interaction of amine or amide residues with the N5 locus of C4a-hydroperoxyflavin also markedly reduces the energy barrier for H<sub>2</sub>O<sub>2</sub> elimination. The interaction of Thr169 and flavin N5-locus shown in TS2 (Figure 4) may be similar to those found in the Bach and Mattevi study.<sup>32</sup> On the basis of our data in Figures 3–4, we propose that a more relaxed H-bond interaction to the flavin N5-H in TS2 when compared to a tighter H-bond interaction in C4a-OOH (bond length of 2.01 Å) is important for allowing H<sub>2</sub>O<sub>2</sub> elimination to occur.

In summary, the combined usage of QM analysis and transient kinetics provides the theoretical basis underlying oxygen activation and the C4a-hydroperoxyflavin stabilization in P2O. Results in this report represent the chemical reaction in a flavoenzyme oxidase that uniquely stabilizes C4a-hydroperoxyflavin. It should be interesting to explore in future studies whether a similar basis holds for monooxygenases in which C4a-hydroperoxyflavin is utilized as a reactive intermediate.

## ■ ASSOCIATED CONTENT

### ● Supporting Information

Reaction catalyzed by P2O. Summary of the relative electronic energies by B3LYP/6-31G(d) and the relative electronic energies with solvation correction by B3LYP/6-311+G(d,p). The expectation value of the total spin angular momentum,  $\langle S^2 \rangle$ . Spin densities of the  $\text{FADH}^{-\text{Free}}\text{:O}_2$ ,  $\text{FADH}\cdot\text{Free}\cdot\text{OOH}$  and  $\text{FADH}\cdot_{\text{Enz}}\cdot\text{OOH}$  complexes. Optimized structures and reaction energies for  $\text{H}_2\text{O}_2$  elimination from C4aOOH on the *re*- and *si*-faces. Effects of temperature on the P2O reaction. Kinetics of the reactions of H167A/H548 variants with  $\text{O}_2$ . Bimolecular rate constants for the imidazole rescue experiments. Coordinates and calculated energies for all structures. This material is available free of charge via the Internet at <http://pubs.acs.org>.

## ■ AUTHOR INFORMATION

### Corresponding Author

pimchai.cha@mahidol.ac.th

### Author Contributions

<sup>‡</sup>T.W. and P.S. contributed equally to this study.

### Funding

This work was supported by The Thailand Research Fund through Grants No. RTA5680001 (to P.C.), MRG5580117 (to P.S.), Development and Promotion of Science and Technology Talents Project DPST Research Grant No. 025/2555 (to P.S.), Center of Excellence for Innovation in Chemistry (PERCH-CIC), Office of the Higher Education and Commission, Ministry of Education (to P.S.), a grant from the Faculty of Science, Mahidol University (to P.C.), and National Science and Technology Development Agency (to T.W.). J.S. received support from The Thailand Research Fund (RSA5580050). N.S.S. is an EPSRC Established Career Fellow and a Royal Society Wolfson Merit Award holder.

### Notes

The authors declare no competing financial interest.

## ■ ACKNOWLEDGMENTS

We thank Bruce A. Palfey, University of Michigan, for critical reading of the manuscript.

## ■ REFERENCES

- (1) Fagan, R. L.; Palfey, B. A. In *Comprehensive Natural Products II: Chemistry and Biology*; Mander, L., Lui, H.-W., Eds.; Elsevier: Oxford, 2010; Vol. 7, pp 37–113.
- (2) Monti, D.; Ottolina, G.; Carrea, G.; Riva, S. *Chem. Rev.* **2011**, *111*, 4111–4140.
- (3) Mirzakulova, E.; Khatmullin, R.; Walpita, J.; Corrigan, T.; Vargas-Barbosa, N. M.; Vyas, S.; Oottikkal, S.; Manzer, S. F.; Hadad, C. M.; Glusac, K. D. *Nat. Chem.* **2012**, *4*, 794–801.
- (4) Leisch, H.; Morley, K.; Lau, P. C. *Chem. Rev.* **2011**, *111*, 4165–4222.
- (5) Fraaije, M. W.; Berkel, W. J. H. v. Flavin-Containing Oxidative Biocatalysts. In *Biocatalysis in the Pharmaceutical and Biotechnology Industries*; Patel, R. N., Ed. CRC Press, Taylor & Francis Group: Boca Raton, FL, 2006; p 181.
- (6) Chaiyen, P.; Fraaije, M. W.; Mattevi, A. *Trends. Biochem. Sci.* **2012**, *37*, 373–380.
- (7) Bruice, T. C. *Isr. J. Chem.* **1984**, *24*, 54–61.
- (8) Eberlein, G.; Bruice, T. C. *J. Am. Chem. Soc.* **1983**, *105*, 6685–6697.
- (9) Massey, V. *J. Biol. Chem.* **1994**, *269*, 22459–22462.
- (10) Klinman, J. P. *Acc. Chem. Res.* **2007**, *40*, 325–333.
- (11) Kommoju, P. R.; Chen, Z. W.; Bruckner, R. C.; Mathews, F. S.; Jorns, M. S. *Biochemistry* **2011**, *50*, 5521–5534.
- (12) Jorns, M. S.; Chen, Z. W.; Mathews, F. S. *Biochemistry* **2010**, *49*, 3631–3639.
- (13) Zhao, G.; Bruckner, R. C.; Jorns, M. S. *Biochemistry* **2008**, *47*, 9124–9135.
- (14) Bruckner, R. C.; Winans, J.; Jorns, M. S. *Biochemistry* **2011**, *50*, 4949–4962.
- (15) McDonald, C. A.; Fagan, R. L.; Collard, F.; Monnier, V. M.; Palfey, B. A. *J. Am. Chem. Soc.* **2011**, *133*, 16809–16811.
- (16) Gadda, G. *Biochemistry* **2012**, *51*, 2662–2669.
- (17) Henderson Pozzi, M.; Fitzpatrick, P. F. *Arch. Biochem. Biophys.* **2010**, *498*, 83–88.
- (18) Sucharitakul, J.; Prongjit, M.; Haltrich, D.; Chaiyen, P. *Biochemistry* **2008**, *47*, 8485–8490.
- (19) Wongnate, T.; Chaiyen, P. *FEBS J.* **2013**, *280*, 3009–3027.
- (20) van der Kamp, M. W.; Mulholland, A. J. *Biochemistry* **2013**, *52*, 2708–2728.
- (21) Groenhof, G. *Methods Mol. Biol.* **2013**, *924*, 43–66.
- (22) Siegbahn, P. E.; Himo, F. *J. Biol. Inorg. Chem.* **2009**, *14*, 643–651.
- (23) Senn, H. M.; Thiel, W. *Angew. Chem., Int. Ed.* **2009**, *48*, 1198–1229.
- (24) Polyak, I.; Reetz, M. T.; Thiel, W. *J. Am. Chem. Soc.* **2012**, *134*, 2732–2741.
- (25) Mata, R. A.; Werner, H. J.; Thiel, S.; Thiel, W. *J. Chem. Phys.* **2008**, *128*, 025104.
- (26) Ridder, L.; Mulholland, A. J.; Rietjens, I. M.; Vervoort, J. *J. Mol. Graphics Modell.* **1999**, *17*, 163–175 and p 214.
- (27) Tian, B.; Strid, A.; Eriksson, L. A. *J. Phys. Chem. B* **2011**, *115*, 1918–1926.
- (28) Tian, B.; Tu, Y.; Strid, A.; Eriksson, L. A. *Chemistry* **2010**, *16*, 2557–2566.
- (29) Wang, X. L.; Quan, J. M. *J. Am. Chem. Soc.* **2011**, *133*, 4079–4091.
- (30) Prabhakar, R.; Siegbahn, P. E.; Minaev, B. F. *Biochim. Biophys. Acta* **2003**, *1647*, 173–178.
- (31) Hernández-Ortega, A.; Lucas, F.; Ferreira, P.; Medina, M.; Guallar, V.; Martínez, A. T. *Biochemistry* **2012**, *51*, 6595–6608.
- (32) Bach, R. D.; Mattevi, A. *J. Org. Chem.* **2013**, *78*, 8585–8593.
- (33) Frisch, M. J.; Trucks, G. W.; Schlegel, H. B.; Scuseria, G. E.; Robb, M. A.; Cheeseman, J. R.; Scalmani, G.; Barone, V.; Mennucci, B.; Petersson, G. A.; Nakatsuji, H.; Caricato, M.; Li, X.; Hratchian, H. P.; Izmaylov, A. F.; Bloino, J.; Zheng, G.; Sonnenberg, J. L.; Hada, M.; Ehara, M.; Toyota, K.; Fukuda, R.; Hasegawa, J.; Ishida, M.; Nakajima, T.; Honda, Y.; Kitao, O.; Nakai, H.; Vreven, T.; Montgomery, J. A.; Peralta, J. E.; Ogliaro, F.; Bearpark, M.; Heyd, J. J.; Brothers, E.; Kudin, K. N.; Staroverov, V. N.; Keith, T.; Kobayashi, R.; Normand, J.; Raghavachari, K.; Rendell, A.; Burant, J. C.; Iyengar, S. S.; Tomasi, J.; Cossi, M.; Rega, N.; Millam, J. M.; Klene, M.; Knox, J. E.; Cross, J. B.; Bakken, V.; Adamo, C.; Jaramillo, J.; Gomperts, R.; Stratmann, R. E.; Yazyev, O.; Austin, A. J.; Cammi, R.; Pomelli, C.; Ochterski, J. W.; Martin, R. L.; Morokuma, K.; Zakrzewski, V. G.; Voth, G. A.; Salvador, P.; Dannenberg, J. J.; Dapprich, S.; Daniels, A. D.; Farkas, O.; Foresman, J. B.; Ortiz, J. V.; Cioslowski, J.; Fox, D. J. *Gaussian 09*, Revision C.01. Gaussian, Inc.: Wallingford CT, 2010
- (34) Becke, A. D. *J. Chem. Phys.* **1993**, *98*, 5648–5652.
- (35) Lee, C.; Yang, W.; Parr, R. G. *Phys. Rev. B* **1988**, *37*, 785–789.
- (36) Stephens, P. J.; Devlin, F. J.; Chabalowski, C. F.; Frisch, M. J. *J. Phys. Chem.* **1994**, *98*, 11623–11627.
- (37) Siegbahn, P. E.; Borowski, T. *Acc. Chem. Res.* **2006**, *39*, 729–738.
- (38) Bauschlicher, C. W. Jr.; Ricca, A.; Partridge, H.; Langhoff, S. R. In *Recent Advances in Density Functional Methods, Part II*; Chong, D. P., Ed.; World Scientific Publishing Co.: Singapore, 1997; Vol. 1, pp 165–228.
- (39) Hariharan, P. C.; Pople, J. A. *Theor. Chim. Acta* **1973**, *28*, 213–222.
- (40) Petersson, G. A.; Al-Laham, M. A. *J. Chem. Phys.* **1991**, *94*, 6081.

- (41) Petersson, G. A.; Bennett, A.; Tensfeldt, T. G.; Al-Laham, M. A.; Shirley, W. A.; Mantzaris, J. *J. Chem. Phys.* **1988**, *89*, 2193.
- (42) Barone, V.; Cossi, M. *J. Phys. Chem. A* **1998**, *102*, 1995–2001.
- (43) Adamo, C.; Barone, V. *J. Chem. Phys.* **1999**, *110*, 6158–6170.
- (44) Hallberg, B. M.; Leitner, C.; Haltrich, D.; Divne, C. *J. Mol. Biol.* **2004**, *341*, 781–796.
- (45) Kujawa, M.; Ebner, H.; Leitner, C.; Hallberg, B. M.; Prongjit, M.; Sucharitakul, J.; Ludwig, R.; Rudsander, U.; Peterbauer, C.; Chaiyen, P.; Haltrich, D.; Divne, C. *J. Biol. Chem.* **2006**, *281*, 35104–35115.
- (46) Isobe, H.; Yamanaka, S.; Kuramitsu, S.; Yamaguchi, K. *J. Am. Chem. Soc.* **2008**, *130*, 132–149.
- (47) Prongjit, M.; Sucharitakul, J.; Wongnate, T.; Haltrich, D.; Chaiyen, P. *Biochemistry* **2009**, *48*, 4170–4180.
- (48) Pitsawong, W.; Sucharitakul, J.; Prongjit, M.; Tan, T. C.; Spadiut, O.; Haltrich, D.; Divne, C.; Chaiyen, P. *J. Biol. Chem.* **2010**, *285*, 9697–9705.
- (49) Sucharitakul, J.; Wongnate, T.; Chaiyen, P. *Biochemistry* **2010**, *49*, 3753–3765.
- (50) Prongjit, M.; Sucharitakul, J.; Palfey, B. A.; Chaiyen, P. *Biochemistry* **2013**, *52*, 1437–1445.
- (51) Eyring, H. *J. Chem. Phys.* **1935**, *3*, 107.
- (52) Winzor, D. J.; Jackson, C. M. *J. Mol. Recognit.* **2006**, *19*, 389–407.
- (53) Wongnate, T.; Sucharitakul, J.; Chaiyen, P. *ChemBioChem* **2011**, *12*, 2577–2586.
- (54) Tan, T. C.; Pitsawong, W.; Wongnate, T.; Spadiut, O.; Haltrich, D.; Chaiyen, P.; Divne, C. *J. Mol. Biol.* **2010**, *402*, 578–594.
- (55) Mattevi, A. *Trends Biochem. Sci.* **2006**, *31*, 276–283.
- (56) Sucharitakul, J.; Wongnate, T.; Chaiyen, P. *J. Biol. Chem.* **2011**, *286*, 16900–16909.
- (57) Tan, T. C.; Haltrich, D.; Divne, C. *J. Mol. Biol.* **2011**, *409*, 588–600.
- (58) Tian, B.; Strid, A.; Eriksson, L. A. *J. Phys. Chem. B* **2011**, *115*, 1918–1926.
- (59) Su, Q.; Klinman, J. P. *Biochemistry* **1999**, *38*, 8572–8581.
- (60) Roth, J. P.; Klinman, J. P. *Proc. Natl. Acad. Sci. U.S.A.* **2003**, *100*, 62–67.
- (61) Thotsaporn, K.; Chenprakhon, P.; Sucharitakul, J.; Mattevi, A.; Chaiyen, P. *J. Biol. Chem.* **2011**, *286*, 28170–28180.
- (62) Orru, R.; Pazmiño, D. E.; Fraaije, M. W.; Mattevi, A. *J. Biol. Chem.* **2010**, *285*, 35021–35028.

## ■ NOTE ADDED AFTER ASAP PUBLICATION

Scheme 3 and Figure 2 contained errors in the version published ASAP December 24, 2013; the correct version reposted December 26, 2013.